A systematic study of impurity ion poloidal rotation and temperature profiles using CXRS in the TJ-II stellarator

J. M.Carmona, K. J. McCarthy, V. Tribaldos, M. Ochando and TJ-II Team

Laboratorio Nacional de Fusión, EURATOM-CIEMAT, E-28040 Madrid, Spain

A detailed analysis of the calibration methods for the new CXRS-DNBI diagnostic system and a systematic study of impurity profiles measured under different plasma conditions have been carried out in TJ-II and presented here. Ion temperatures profiles tend to be flat in the measured region, showing correlation between ECRH power, averaged electron densities and the Ti value. Transition of poloidal velocities from ion to electron diamagnetic direction when increasing the line averaged electron density ($<n_e>$) was confirmed, agreeing with previous works. As line averaged density was considered to be the driver-parameter of this transition, shots with the same electron density and different ECRH power were compared to highlight other contributions as T_e. A change in ion temperature and poloidal rotation direction is found when comparing these shots, suggesting that the plasma collision frequency ($\sim n_e T_e^{-3/2}$) tends to control the dynamics in TJ-II, giving a clearer description of the trigger mechanism. First experimental evidence in TJ-II that the shear point for impurity velocities moves outwards when increasing n_e, is also presented.

Keywords: Charge exchange spectroscopy, temperature profiles, poloidal rotation

1. Introduction

Spatially resolved measures of ion temperature and poloidal rotation are important for the understanding of plasma dynamics. For this reason, an active charge-exchange recombination spectroscopy (CXRS) diagnostic, based around a diagnostic neutral beam injector (DNBI) and a bidirectional (two vertical opposing views) multi-channel spectroscopic system [1, 2], has been set-up on the TJ-II, a four-period [3], low magnetic shear, stellarator. It provides 5 ms long pulses, up to two per discharge, of neutral hydrogen accelerated to 30 keV with equivalent current of 3.3 equ. A. The bidirectional diagnostic is designed to measure Doppler shifts and widths of the C VI line at λ = 529.06 nm in up to 3 arrays of 12 channels with ~1 cm spatial resolution across the plasma minor radius. The light dispersion element is a Holospec spectrograph with three 100 μm curved entrance slits (these are curved to compensate for its short focal length) and a transmission grating sandwiched between two BK7 prisms. It provides a focal-plane dispersion of ~1.15 nm/mm at 529 nm. Moreover, a narrow bandpass filter (2.0±0.5 nm at full-width at half-maximum FWHM) centred on 529 nm prevents spectral overlapping from the multiple fibre arrays at the image plane. The set-up includes a high-efficiency back-illuminated CCD camera and fast mechanical shutter (=4.5 ms time window). With on-chip binning, multiple spectra can be collected during discharges (=300 ms). Finally, fibre alignment was performed by illuminating each fibre bundle with a bright light source and observing, through an unused viewport, the orientation and location of the resultant bright spots with respect to markings on the inside of the opposing vacuum flange. In this way, the sightlines through plasmas can be determined using a cross-sectional machine drawing and magnetic configuration maps. Hence, when compared with the neutral beam geometry the normalized radius, r/a, corresponding to each beam/line-of-sight interaction volume is found. Finally, for the magnetic configuration used in this study, 100-44-64, the viewing system covered the plasma minor radius from r/a= 0.3 to 0.85.

2. Experimental details

2.1. Diagnostic set-up

The TJ-II is a four field period heliac type stellarator ($B(0)$ = 1.2 T, R = 1.5 m, $<a>$ = 0.22 m) designed to explore a wide rotational transform range ($0.9 = \iota(0)/2\pi = 2.2$) in low, negative shear configurations ($\Delta\iota/\iota < 6\%$). The experiments reported here were carried out in electron cyclotron resonance heated (ECRH) plasmas (P_{ECRH}= 300 – 500 kW, 53.2 GHz, 2nd harmonic, X-mode polarization, $t_{discharge}$ = 250 ms) with hydrogen as the working gas [3] and lithium coated walls (previously boronized). No auxiliary NBI heating was provided. As a result, central electron densities and temperatures up to ~10^{19} m^{-3} and ~1.5 keV respectively were achieved. The strong reduction in impurities concentration (i.e. carbon) due to the wall-coating results in reduced impurity photon fluxes thereby requiring efficient detection procedures. Nevertheless, the use of a high-throughput spectrograph and an efficient CCD detector made the goal of

author's e-mail: jm.carmona@ciemat.es

measuring in such conditions possible.

2.2. Instrument calibration

Special attention has been given to wavelength calibration and instrumental function determination. Calibration for each individual fibre was done in order to detect small variations in the alignment of the fibres and in the FWHM of spectral lines. Spectra were captured between discharges using a retractile pencil-type Neon lamp positioned between the lens and fibre bundle head.

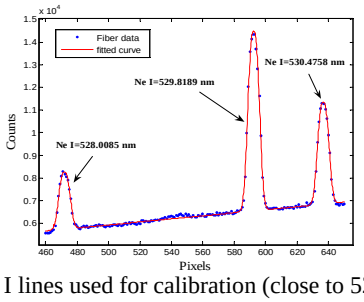

Fig.1 Ne I lines used for calibration (close to 529 nm)

Wavelength calibration was performed using a second order (polynomial) fit to the three nearby Ne I spectral lines (figure-1). As spectra are recorded simultaneously for all fibres, fine corrections can be made for any nonlinear dispersion present in the spectrometer or displacement errors in the entrance slits. Next, the instrument function was determined from the same spectra using a Gaussian function fitting. It was found to be ~7.6 pixels (~1.14 Å) and ~6.3 pixels (~0.95 Å) for the mid fibres of the upper and lower arrays respectively (figure-1 in [2]) and to vary along the fibre array.

Figure-2a illustrates the variation in FWHM along the lower array. Such a variation is inherent to the set-up of this instrument [4]. Part of it may also be due to inaccuracies when manufacturing the slits (a similar behaviour is observed for the upper array).

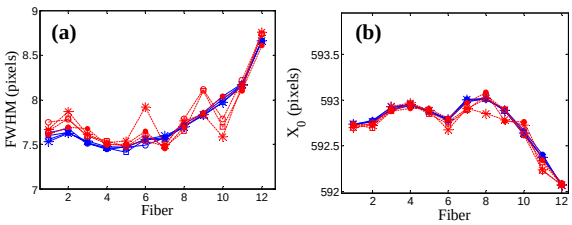

Fig.2 Variation of (a) instrumental FWHM (b) on fibre position along the middle fibres for robust (red) and non-robust (blue) methods. The symbols represent different frames.

It should be noted that the neon lines fits were made using a non-linear least squares method based on trust-region algorithms. For this, comparisons between different fitting methods were made (*i.e.* robust and non-robust). See figure-2a (FWHM) and figure-2b (central position). In general, robust algorithms are considered preferable to non-robust ones, as the former are less sensitive to outlier points (points numerically distant from the rest that can lead to misleading fits). However, here it was found that robust fits show significant fibre-to-fibre variations for both FWHMs (figure-2a) and line centres whilst non-robust fits (figure-2b) are more stable. Indeed, in certain situations robust methods may be preferable, *e.g.* for single Gaussian fits, but they prove to be weak when multiple Gaussian fits are performed. Hence, the non-robust method was chosen as the fitting method.

2.3. Active and passive signal treatment

CXRS is widely employed to obtain spatially resolved measurements, although it presents several challenges. For instance, contributions to measured signals from ionized impurities (called the *cold component* or *passive* signal) must be removed since it is a non localized emission. Also plasma conditions should remain constant along a discharge, or discharges should be reproducible (shot to shot technique), so that the active signal can be obtained by subtraction, i.e. (A+P)-(P) =A. See figure-3. For the data presented here, both techniques were employed.

2.4. Data Analysis

Once the instrumental and calibration functions have been obtained for each fibre using the neon lamp, fits to the line of interest (i.e. C VI @ 529.06 nm) can be made so that Doppler shifts and widths can be estimated together with errors. Ion temperatures and velocities are deduced from the usual relations:

$$T_i = 1.68 \cdot 10^8 A \left(\frac{\Delta l^2_{fwhm} - \Delta l^2_{instrum}}{l_0^2} \right)$$
$$v = \left(\frac{l - l_0}{l_0} \right) c \qquad (1)$$

where A is the mass of the ion [amu], $\Delta\lambda_{fwhm}$ the measured full width at half maximum (FWHM), $\Delta\lambda_{instrum}$ the instrument FWHM, λ and λ_0 are the measured and the unshifted central wavelength of line under consideration respectively and *c* the speed of light. For this work, a wavelength of λ_0=529.06 nm is taken as reference value in equation (1) (the line centre depends weakly on plasma conditions).

2.4.1. Fine structure corrections to C VI data

A clear asymmetry was observed about measured spectra line data. This was interpreted as arising from fine structures in the transitions in this hydrogen-like ion [5, 6]. Indeed, there are up to 13 possible lines with different intensities depending on plasma conditions. Such fine structure give rise to the tail observed on the short

wavelength side that results in apparent line broadening, and hence overestimated ion temperatures.

Thus, in order to correct for this a multi-Gaussian fit, using relative intensity ratios between fine structure components, was employed here. Finally, after careful analysis and consideration, contamination by a nearby O VI line was excluded as there is a strong oxygen reduction due to the boron and lithium coated walls.

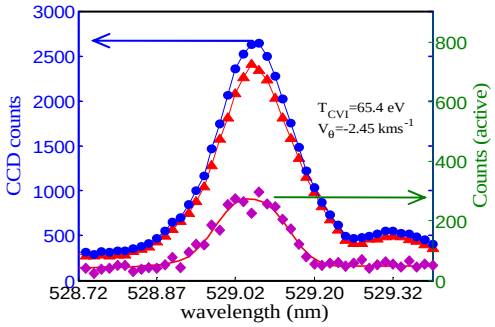

Fig.3 Spectra of subsequent CCD frame at r/a=0.55, showing CX with C^{+6}. Diamonds, triangles and dots are active, passive and active+passive signals respectively. A fit to the active CVI line is also shown.

3. CXRS profiles and discussion

For the study undertaken, hydrogen plasmas with lithium coated walls were made, lasting =250 ms, with line averaged electron densities between 0.4 x 10^{19} m^{-3} and 0.9 x 10^{19} m^{-3} heated only with ECRH. In order to separate active from active plus passive C VI signals only discharges with almost constant electron density and temperature were used.

3.1. Measurements of ion temperature and poloidal rotation profiles

First CXRS profiles of measured ion temperatures for two discharges with 395 kW of ECRH but different line averaged electron densities (n_e) are shown in figure-4. In these plots, the measured C^{6+} impurity temperature is found to be higher for the discharge with lower n_e. Previous studies carried out in the TJ-I tokamak for C^{4+} ions [7] and in the TJ-II for several different ions (C^{4+} and Fe^{15+}, etc…) [8] using passive spectroscopy, reported a similar behaviour. Then, the anomalous temperatures were attributed to non-thermal velocity contributions.

It is apparent from figure-4 that ion temperature profiles are relatively flat and begin to drop for r/a=0.7. Temperature values are measured between 50 and 150 eV, in accordance with the weak collisional coupling for these densities.

For the same shots, poloidal rotation profiles are shown in figure-5. A clear transition from ion to electron diamagnetic direction can be seen.

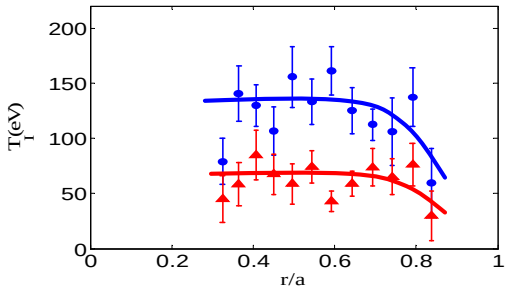

Fig.4. Ion temperature profiles obtained for two discharges with P_{ecrh}=395 kW and line averaged densities n_e=0.42 x 10^{19} m^{-3} (dots) and n_e=0.90 x 10^{19} m^{-3} (triangles) as a function of normalized plasma radius. Lines are plotted to aid the reader.

For lower line-averaged electron densities (<n_e>), C^{6+} ions appear to rotate poloidally in the ion diamagnetic direction whereas at higher values this changes towards the electron diamagnetic direction.

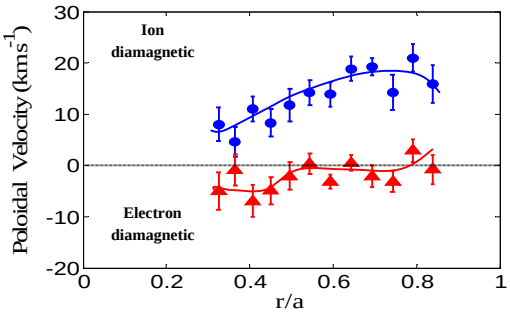

Fig.5. Poloidal rotation profiles of C^{6+} for shots included in figure 4. Lines are plotted to aid the reader.

An in depth analysis of this change in rotation has been performed from a detailed density scan with CXRS diagnostic. This is supported below.

3.2. Density scan

A density scan (from 0.4 to 0.92 x 10^{19} m^{-3}) for 395 kW of ECRH has been made and the poloidal velocities measured are presented. See figure-6. The impurity poloidal velocities show a change of direction as the line averaged electron density is increased, from ion to electron diamagnetic direction (transition from electron to ion root). Such behaviour was also reported in the TJ-II for passive measurements of CV ion temperatures previously [9] thereby providing us with confidence of these CXRS measurements.

Note that, the transition point (i.e. where the poloidal velocity~0) moves towards the edge (from r/a~0.4/0.55 to r/a~0.7/0.8) as <n_e> increases from ~0.57 to ~0.77 x 10^{19} m^{-3}.

This is the first experimental evidence for C^{6+} that the shear point of impurity ion rotation moves outwards in TJ-II with increasing electron density.

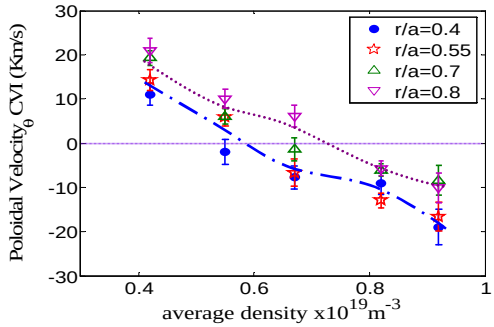

Fig.6. Change on C^{+6} poloidal velocity from ion to electron diamagnetic direction while increasing line averaged electron density. This is plotted for different normalized plasma radii r/a. Lines are plotted to aid the reader.

3.3. Profiles under different P_{ECRH}

Ion temperatures and poloidal rotation profiles are compared for different ECRH conditions. A comparison between shots with a fixed $<n_e>$ and P_{ECRH} of 400 kW and 500 kW are presented. See figure-7 and figure-8.

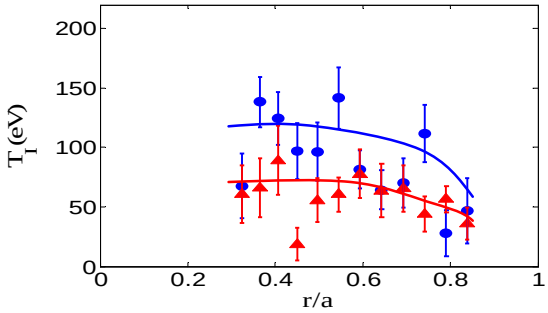

Fig.7. C^{6+} temperature profiles for 400 kW (dots) and 500 kW (triangles) of P_{ECRH} and the same line averaged density $<n_e>=0.6 \times 10^{19}$ m^{-3}, showing lower temperatures for higher P_{ECRH}.

In these figures, lower temperatures are found for higher P_{ECRH} at fixed $<n_e>$. The better coupling between electrons and ions for lower P_{ECRH} (lower T_e) and the decreasing impurity confinement times [10] are expected to cause the increase in temperature in these plasmas ECRH.

A simple power balance equation can help to explain the measured profiles. This is given by

$$\frac{dT_b}{dt} = n_E^{b/e}(T_e - T_b) - \frac{T_b}{t_E^b} \qquad (2)$$

where $\nu_E^{b/e} \sim n_e T_e^{-3/2}$. Better coupling (higher collision frequency $\nu_E^{b/e}$) between ion and electron species (increasing n_e or decreasing T_e) give rise to an increase of ion temperature. With fixed $<n_e>$ and varying T_e (power scan), or vice versa (density scan) ion temperatures can be expected to vary, i.e. increasing when (a) T_e decreases (fixed $<n_e>$) or (b) $<n_e>$ increases (fixed T_e).

From this, the impurity rotation profile in the region accessible, is seen to shift to the electron diamagnetic direction as the injected P_{ECRH} is increased.

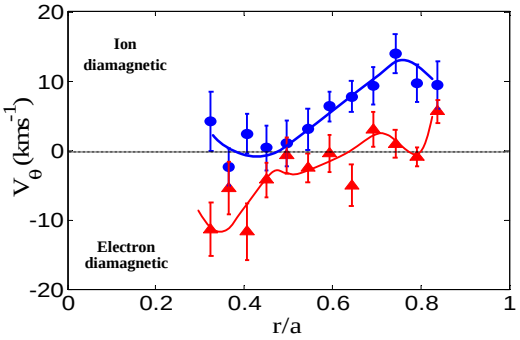

Fig.8. C^{6+} rotation profiles for 400 kW (dots) and 500 kW (triangles) of P_{ECRH} and line-averaged electron density $<n_e>=0.60 \times 10^{19}$ m^{-3}.

4. Summary

A systematic study on the calibration system had been carried out to characterize system capabilities and determine the best data-analysis procedure. Ion temperature and poloidal rotation profiles were measured under different plasma conditions. As seen from experiments, the change from ion to electron diamagnetic direction and ion temperatures depends on $<n_e>$ and T_e, suggesting that the control-parameter is the plasma collision frequency $\nu_E^{b/e} \sim n_e T_e^{-3/2}$. Experimental evidence of displacement with electron density of the shear point for C^{6+} in ECR heated plasmas is reported for the first time in TJ-II.

References

[1] K.J. McCarthy *et al.*, Rev. Sci. Instrum. 75 (2004) 3499
[2] J.M. Carmona *et al.*, Rev. Sci. Instrum. 77 (2006) 10F107
[3] E. Ascasíbar *et al.*, Fusion Eng. Des. 56-57, (2001) 145
[4] R. E. Bell *et al.*, Rev. Sci. Instrum. 75 (2004) 4158
[5] R. J. Fonck, Phys. Rev. A 29, (1984) 3288.
[6] K. Ida *et al.*, Rev. Sci. Instrum. 71 (2000) 2360.
[7] B. Zurro *et al.*, Phys. Rev. Lett., 69 (1992) 2919
[8] K. J. McCarthy *et al.*, Europhys. Lett. 63 (2003) 49-55
[9] B. Zurro *et al.*, Fusion Sci. Technol. 50 (2006) 419-427
[10] R. Burhenn *et al.*, Fusion Sci. Technol. 46 (2006) 115